

Leading twist nuclear shadowing: uncertainties, comparison to experiments and higher twist effects

L. Frankfurt

*Nuclear Physics Dept.,
School of Physics and Astronomy,
Tel Aviv University,
69978 Tel Aviv, Israel
E-mail: frankfur@lev.tau.ac.il*

V. Guzey

*Institut für Theoretische Physik II,
Ruhr-Universität Bochum, D-44780 Bochum, Germany
E-mail: vadim.guzey@tp2.ruhr-uni-bochum.de*

M. Strikman

*Department of Physics,
the Pennsylvania State University,
State College, PA 16802, USA
E-mail: strikman@phys.psu.edu*

Abstract

Using a leading twist approach to nuclear shadowing, which is based on the relationship between nuclear shadowing and diffraction on a nucleon, one can calculate next-to-leading order nuclear parton distribution functions (nPDFs) and structure functions in the region $0.2 > x > 10^{-5}$ and $Q^2 \geq 4 \text{ GeV}^2$. We update our calculations of nPDFs with an emphasis on theoretical uncertainties of our predictions. We find that the contribution of large diffractive masses $\gg Q^2$, which is an analog of the triple Pomeron exchange, becomes significant only for $x \leq 10^{-4}$. Comparing our predictions to the available fixed-target nuclear DIS data, we demonstrate that the data at small x and Q^2 contain significant higher twist effects hindering the extraction of nPDFs from that data. Also, we find that the next-to-leading order effects in the nuclear structure function F_2 are quite sizable.

Within the same formalism, we also study the impact parameter dependence of nPDFs.

PACS numbers: 24.85.+p, 13.60.Hb

I. INTRODUCTION

One way to analyze the microscopic structure of atomic nuclei is to study the distribution of quarks and gluons, as well as their correlations, in nuclei. These nuclear parton distribution functions (nPDFs) can be accessed using various deep inelastic scattering (DIS) processes: Inclusive scattering of leptons, high-mass dimuon production using proton beams, exclusive electroproduction of vector mesons. None of the above processes determines nPDFs comprehensively, only taken together do these experiments provide stringent constraints for nPDFs.

The discussion of the present paper is centered around the nuclear effects of nuclear shadowing and enhancement, which affect nPDFs at small values of Bjorken variable x , $10^{-5} \leq x \leq 0.2$. Nuclear shadowing of nPDFs is developing into an increasingly important subject because it is involved in the interpretation of the RHIC data on jet production, evaluation of hard phenomena in proton-nucleus and nucleus-nucleus collisions at the LHC, estimates of the black limit scattering regime in DIS, etc.

The major obstacle that hinders our deeper knowledge of nPDFs at small x is that, up to the present day, all experiments aiming to study nPDFs are performed with fixed (stationary) nuclear targets. In these data, the values of x and Q^2 are strongly correlated and one measures nPDFs essentially along a curve in the $x - Q^2$ plane rather than exploring the entire plane. Moreover, for $Q^2 > 1 \text{ GeV}^2$, the data cover the region $x > 5 \times 10^{-3}$, where the effect of nuclear shadowing is just setting in. As a result, when one attempts to globally fit the available data by modeling nPDFs at some initial scale Q_0^2 and then performing QCD evolution, various groups [1, 2, 3, 4, 5] produce significantly different results [6].

An alternative to the fitting to the data is to combine the Gribov theory [7], which relates the nuclear shadowing correction to the total hadron-deuteron cross section to the cross section of diffraction off a free nucleon, and the Collins factorization theorem [8] for hard diffraction in DIS. The resulting leading twist theory of nuclear shadowing was developed in [9] and elaborated on in [10].

The Gribov theory has been applied to the description of nuclear shadowing for many years. First it was done in the region of small Q^2 , where generalized vector dominance model gives a good description of diffraction, see review in [11], and later in deep inelastic region, where large diffractive masses $M^2 \propto Q^2$ dominate [12]. A number of successful model

calculations were performed [13, 14, 15, 16, 17, 18, 19, 20, 21] before the experimental data from HERA became available. A calculation constrained to reproduce the HERA data using the Gribov theory was presented in [22]. It focuses on the calculation of nuclear shadowing for F_2^A at intermediate Q^2 where leading and higher twist effects are equally important. A fair agreement of the data with the Gribov theory has been found. However, this approach does not involve the use of the Collins factorization theorem and, hence, does not address nPDFs (see a detailed comparison in Sect. IV).

The present work updates the calculation of nPDFs of [10] with an emphasis on the theoretical unambiguity and accuracy of the predictions and makes a comparison to fixed-target nuclear DIS data. In particular, we demonstrate that

- The leading twist theory of nuclear shadowing and QCD analysis of hard diffraction at HERA enable one to predict in a model-independent way the next-to-leading order nPDFs for $10^{-5} \leq x \lesssim 10^{-2}$ with 30% accuracy, Fig. 6. For larger x , $10^{-2} \leq x \leq 0.1 - 0.2$, there appears an additional effect of nuclear antishadowing that requires modeling and whose uncertainty is larger.
- The failure to describe the available fixed-target data for $0.003 < x < 0.02$ indicates the presence of significant higher twist effects in the data, see Fig. 10. This signals that any leading twist QCD analysis of the available data is unreliable for $0.003 < x < 0.02$.
- The next-to-leading order (NLO) effects in the inclusive nuclear structure function F_2 are found to be quite sizable. This means that it is not selfconsistent to use the leading order parametrizations of nPDFs in the NLO QCD calculations, see Fig. 13.

In short, the main goals of the paper are to give a concise summary of the leading twist theory of nuclear shadowing, to assess the theoretical uncertainties of the resulting predictions and to make a comparison to nuclear DIS data. We attempted to give a selfcontained presentation and, hence, this paper can be rightfully considered as a *guide* to leading twist nuclear shadowing.

II. LEADING TWIST THEORY OF NUCLEAR SHADOWING

In this section, we review the leading twist approach to nuclear shadowing developed in [9] and further elaborated on in [10].

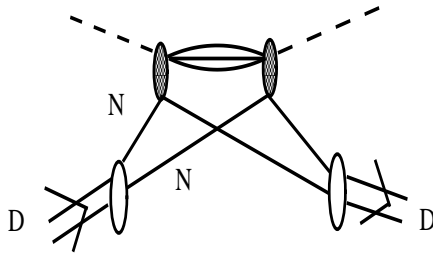


FIG. 1: Gribov's theorem [7]: The forward hadron-deuteron rescattering amplitude, which gives rise to nuclear shadowing, is proportional to the differential hadron-nucleon diffractive cross section.

The approach is based on the 1969 work by V. Gribov [7], where the following theorem was proven. Let us consider hadron-deuteron scattering at high energies within the approximation that the radius of the deuteron is much larger than the range of the strong interaction. Then the shadowing correction to the total cross section is expressed in terms of the differential diffractive hadron-nucleon cross section. This is demonstrated in Fig. 1: The forward hadron-deuteron rescattering amplitude giving rise to the nuclear shadowing correction contains the hadron-nucleon diffractive amplitude (denoted by the shaded blob) squared.

The relationship between nuclear shadowing and diffraction was used in the analysis of parton densities of deuterium and other nuclei by Frankfurt and Strikman in [9]. For deuterium and other sufficiently light (low nuclear density) nuclei, nuclear shadowing and diffraction on the nucleon are related in a model-independent way using the Gribov theorem[50].

A generalization to heavy nuclei involves certain modeling of multiple rescattering contributions, which, however, is under control [23]. Below we shall recapitulate the derivation

of the leading twist nuclear shadowing for nPDFs, which can be carried out in three steps.

Step 1. The shadowing correction arising from the coherent interaction with any two nucleons of the nuclear target with the atomic mass number A , $\delta F_{2A}^{(2)}$ (the superscript (2) serves as a reminder that only the interaction with two nucleons is accounted for), is expressed in terms of the proton diffractive structure function $F_2^{D(4)}$ (the superscript (4) indicates dependence on four kinematic variables) as a result of the generalization of the Gribov result for deuterium (see also Ref. [11]). This does not require decomposition over twists and is therefore valid even for the case of real photon interactions. The shadowing correction $\delta F_{2A}^{(2)}$ reads [51]

$$\delta F_{2A}^{(2)}(x, Q^2) = \frac{A(A-1)}{2} 16\pi \mathcal{R}e \left[\frac{(1-i\eta)^2}{1+\eta^2} \int d^2b \int_{-\infty}^{\infty} dz_1 \int_{z_1}^{\infty} dz_2 \int_x^{x_{\mathcal{P},0}} dx_{\mathcal{P}} \right. \\ \left. \times F_2^{D(4)}(\beta, Q^2, x_{\mathcal{P}}, t) \Big|_{t=t_{\min}} \rho_A(b, z_1) \rho_A(b, z_2) e^{ix_{\mathcal{P}} m_N (z_1 - z_2)} \right], \quad (1)$$

with η the ratio of the real to imaginary parts of the diffractive scattering amplitude; z_1 , z_2 and \vec{b} the longitudinal (in the direction of the incoming virtual photon) and transverse coordinates of the nucleons involved (defined with respect to the nuclear center); β , $x_{\mathcal{P}}$ and t the usual kinematic variables used in diffraction. Throughout this work, we use $\beta = x/x_{\mathcal{P}}$. Equation (1) uses the fact that the t -dependence of the elementary diffractive amplitude is much weaker than that of the nuclear wave function, and, hence, $F_2^{D(4)}$ can be approximately evaluated at $t = t_{\min} \approx 0$. All information about the nucleus is encoded in the nucleon distributions $\rho_A(b, z_i)$. Finally, $x_{\mathcal{P},0}$ is a cut-off parameter ($x_{\mathcal{P},0} = 0.1$ for quarks and $x_{\mathcal{P},0} = 0.03$ for gluons), which will be discussed later in the text.

The origin of all factors in Eq. (1) can be readily seen by considering the corresponding forward double rescattering Feynman diagram (see Fig. 2), which accounts for the diffractive production of intermediate hadronic states by the incoming virtual photon:

- The combinatoric factor $A(A-1)/2$ is the number of the pairs of nucleons involved in the rescattering process.
- The factor 16π provides the correct translation of the differential diffractive to the total rescattering cross section (see the definition later), as required by the Glauber theory [11, 25].
- The factor $(1-i\eta)^2/(1+\eta^2)$ is a correction for the real part of the diffractive scattering amplitude \mathcal{A} . Since the shadowing correction is proportional to $(Im\mathcal{A})^2$, while the total

diffractive cross section is proportional to $|\mathcal{A}|^2$, the factor $(1 - i\eta)^2/(1 + \eta^2)$ emerges naturally, when one expresses nuclear shadowing in terms of the total diffractive cross section (diffractive structure function).

- The integration over the positions of the nucleons is the same as in the Glauber theory. Similarly, because the recoil of the nucleons is neglected (the transverse radius of the elementary strong amplitude is much smaller than the scale of the variation of the nuclear density), both involved nucleons have the same transverse coordinate \vec{b} .
- The integration over x_P represents the sum over the masses of the diffractively produced intermediate states.
- In order to contribute to nuclear shadowing (not to break up the nucleus in its transition from the $|\text{in}\rangle$ -state to the $\langle\text{out}|$ -state), the virtual photon should interact with the nucleons diffractively. The product of the two diffractive amplitudes (depicted as shaded blobs in Fig. 2) gives the diffractive structure function of the proton $F_2^{D(4)}$. Also note that we do not distinguish between diffraction on the proton and neutron in the present work, as the corresponding diffractive amplitudes are equal at small x .
- The effect of the nucleus is given by the nucleon densities $\rho_A(b, z_i)$. For the sufficiently heavy nuclei that we consider, nucleon-nucleon correlations can be neglected and the nuclear wave function squared can be approximated well by the product of individual $\rho_A(b, z_i)$ for each nucleon (the so-called independent particle approximation).
- The factor $e^{ix_P m_N(z_1 - z_2)}$ is a consequence of the propagation of the diffractively produced intermediate state between the two nucleons involved.

Step 2. The QCD factorization theorems for inclusive [26] and hard diffractive DIS [8] can be used to relate the structure functions in Eq. (1) to the corresponding – inclusive and diffractive – parton distribution functions. Since the coefficient functions (hard scattering parts) are the same for both inclusive and diffractive structure functions, the relation between the shadowing correction to nPDFs and the proton diffractive parton distribution functions (PDFs) is given by an equation similar to Eq. (1). The shadowing correction to the nPDF of flavor j , $f_{j/A}$, $\delta f_{j/A}^{(2)}$, is related to the proton (nucleon) diffractive PDF $f_{j/N}^{D(4)}$ of the same

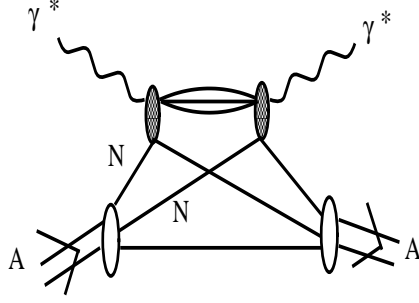


FIG. 2: The forward γ^* -nucleus rescattering amplitude that gives the principal contribution to nuclear shadowing.

flavor

$$\delta f_{j/A}^{(2)}(x, Q^2) = \frac{A(A-1)}{2} 16\pi \mathcal{R}e \left[\frac{(1-i\eta)^2}{1+\eta^2} \int d^2b \int_{-\infty}^{\infty} dz_1 \int_{z_1}^{\infty} dz_2 \int_x^{x_{P,0}} dx_{\mathbb{P}} \right. \\ \left. \times f_{j/N}^{D(4)}(\beta, Q^2, x_{\mathbb{P}}, t)|_{t=t_{\min}} \rho_A(b, z_1) \rho_A(b, z_2) e^{ix_{\mathbb{P}} m_N (z_1 - z_2)} \right]. \quad (2)$$

Equation (2) is very essential in several ways. Firstly, it enables one to evaluate nuclear shadowing for each parton flavor j separately. Secondly, since the diffractive PDFs obey leading twist QCD evolution, so does the shadowing correction $\delta f_{j/A}^{(2)}$. This explains why the considered theory can be legitimately called the leading twist approach. Since Eq. (2) is based on the QCD factorization theorem, it is valid to all orders in α_s . Hence, if $f_{j/N}^{D(4)}$ is known with the next-to-leading order (NLO) accuracy, as is the case for the used H1 parameterization for $f_{j/N}^{D(4)}$, we can readily make predictions for NLO nPDFs.

Step 3. Equation (2) is derived in the approximation of the low nuclear thickness, and it takes into account only the interaction with two nucleons of the target. The effect of the rescattering on three and more nucleons can be taken into account by introducing the

attenuation factor $T(b, z_1, z_2)$ (see for example [11]),

$$T(b, z_1, z_2) = e^{-(A/2)(1-i\eta)\sigma_{\text{eff}}^j \int_{z_1}^{z_2} dz \rho_A(b, z)}, \quad (3)$$

where the meaning of σ_{eff}^j should become clear after the following discussion. Let us consider sufficiently small values of Bjorken variable x such that the factor $e^{ix_{\mathbb{P}} m_N(z_1 - z_2)}$ in Eq. (2) can be neglected. Then, introducing σ_{eff}^j as

$$\sigma_{\text{eff}}^j(x, Q^2) = \frac{16\pi}{f_{j/N}(x, Q^2)(1 + \eta^2)} \int_x^{x_{\mathbb{P},0}} dx_{\mathbb{P}} f_{j/N}^{D(4)}(\beta, Q^2, x_{\mathbb{P}}, t)|_{t=t_{\min}}, \quad (4)$$

Eq. (2) can be written in the form equivalent to the usual Glauber approximation

$$\begin{aligned} \delta f_{j/A}^{(2)}(x, Q^2) &\approx \frac{A(A-1)}{2} (1 - \eta^2) \sigma_{\text{eff}}^j(x, Q^2) f_{j/N}(x, Q^2) \\ &\times \int d^2b \int_{-\infty}^{\infty} dz_1 \int_{z_1}^{\infty} dz_2 \rho_A(b, z_1) \rho_A(b, z_2), \end{aligned} \quad (5)$$

where $f_{j/N}$ is the proton inclusive PDF. Therefore, it is clear that thus introduced σ_{eff}^j has the meaning of the rescattering cross section, which determines the amount of nuclear shadowing in the approximation of Eq. (5). Hence, it is natural to assume that the same cross section describes rescattering with the interaction with three and more nucleons, as postulated by the definition of the attenuation factor $T(b, z_1, z_2)$ by Eq. (3). In the language of Feynman diagrams, the assumed form of the attenuation factor implies that the diffractively produced intermediate state rescatters without a significant change of mass with the same cross section on all remaining nucleons of the target, as depicted in Fig. 3 for the case of the triple scattering. The approximation of elastic rescattering is not important at small enough x where longitudinal distances are much larger than the nuclear size, see discussion below.

Corrections to the elastic rescattering approximation can be estimated by taking into account the effects of fluctuations of the strength of the rescattering interaction. Modeling of these effects was performed in [23] with the conclusion that for a wide range of cross section fluctuations, the reduction of nuclear shadowing (for fixed σ_{eff}) remains a rather small correction for all nuclei.

After introducing the attenuation factor into Eq. (2), the complete expression for the shadowing correction, $\delta f_{j/A}$, becomes

$$\begin{aligned} \delta f_{j/A}(x, Q^2) &= \frac{A(A-1)}{2} 16\pi \mathcal{R} e \left[\frac{(1-i\eta)^2}{1+\eta^2} \int d^2b \int_{-\infty}^{\infty} dz_1 \int_{z_1}^{\infty} dz_2 \int_x^{x_{\mathbb{P},0}} dx_{\mathbb{P}} \right. \\ &\times f_{j/N}^{D(4)}(\beta, Q^2, x_{\mathbb{P}}, t_{\min}) \rho_A(b, z_1) \rho_A(b, z_2) e^{ix_{\mathbb{P}} m_N(z_1 - z_2)} e^{-(A/2)(1-i\eta)\sigma_{\text{eff}}^j \int_{z_1}^{z_2} dz \rho_A(b, z)} \left. \right]. \end{aligned} \quad (6)$$

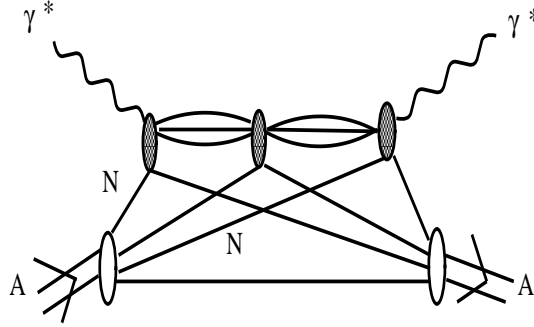


FIG. 3: The forward γ^* -nucleus triple scattering amplitude.

This is our master equation (see also Eq. (14)). It contains several sources of model-dependence and theoretical ambiguity. First, the attenuation factor $T(b, z_1, z_2)$ assumes that multiple rescatterings can be described by a single rescattering cross section[52] σ_{eff}^j , i.e. cross section fluctuations are neglected in the interaction with three and more nucleons. Second, the necessity to introduce the parameter $x_{\mathbb{P},0}$ is a consequence of the fact that Eq. (6) applies only to the region of nuclear shadowing: The transition to the region of the enhancement of nPDFs should be modeled separately. This is the role of the parameter $x_{\mathbb{P},0}$. Third, there are experimental uncertainties in the determination of the diffractive PDFs $f_{j/N}^{D(4)}$ which we use as an input in Eq. (6).

Equation (6) defines the input nPDFs for the DGLAP evolution equations. As a starting evolution scale Q_0^2 , we take $Q_0^2 = 4 \text{ GeV}^2$: This is the lowest value of Q^2 of the H1 diffractive fit [27]. Nuclear PDFs at $Q^2 > Q_0^2$ are obtained using the NLO QCD evolution equations. Therefore, we predict that nuclear shadowing is a leading twist phenomenon.

In the small- x limit, which for practical purposes means $x < 10^{-3}$, the factor $e^{ix_{\mathbb{P}}m_N(z_1-z_2)}$ in Eq. (6) can be safely omitted, which results in a significant simplification of the master

formula (after integration by parts two times)

$$\delta f_{j/A}(x, Q^2) = \frac{2(1 - 1/A) f_{j/N}(x, Q^2)}{\sigma_{\text{eff}}^j} \text{Re} \left(\int d^2b (e^{-LT(b)} - 1 + LT(b)) \right), \quad (7)$$

where $L = A/2(1 - i\eta) \sigma_{\text{eff}}^j$; $T(b) = \int_{-\infty}^{\infty} dz \rho_A(b, z)$.

In the heavy nucleus limit ($A \rightarrow \infty$) and at fixed σ_{eff} ,

$$\frac{f_{j/A}(x, Q^2)}{A f_{j/N}(x, Q^2)} = 1 - \frac{\delta f_{j/A}(x, Q^2)}{A f_{j/N}(x, Q^2)} = \frac{2\pi R_A^2}{A \sigma_{\text{eff}}^j}. \quad (8)$$

III. PARAMETERS AND UNCERTAINTIES OF THE METHOD

The master equation (6) uses as the input the information on hard diffraction in DIS on the proton, which was measured at HERA by ZEUS [28] and H1 [29] collaborations. We use the H1 parameterization of $f_{j/N}^{D(3)}$ [27] (note the superscript (3) indicating that the t -dependence of diffraction is not measured), which is based on the QCD analysis of the 1994 H1 data [29] (we use model 4, see Appendix A of Ref. [10]). The choice of the H1 parameterization is motivated by the following observations:

- It is available in an easily accessible and usable form, see [27] and also Appendix A of Ref. [10].
- The diffractive jet production in DIS at HERA data [30] is best described by the H1 parameterization. The fit of Alvero, Collins, Terron and Whitmore [31] somewhat overestimates the data. Another available in the literature parameterization, that of Hautmann, Kunszt and Soper [32], is not based on the detailed fit to the available diffractive data.
- The 1994 H1 fit is in fair agreement with the most recent 1997 H1 data [33]. However, the 1997 H1 data indicates that the gluon distribution of the 1994 fit is too large by about 25%. Hence, in our anylysis we multiplied the gluon diffractive distribution of [27] by 0.75.

Since the diffractive PDF $f_{j/N}^{D(4)}$ enters Eq. (6) at $t \approx 0$, one has to assume a certain t -dependence in order to be able to use the H1 results for the t -integrated $f_{j/N}^{D(3)}$. The common choice is to assume that

$$f_{j/N}^{D(4)}(\beta, Q^2, x_P, t) = e^{B_j t} f_{j/N}^{D(4)}(\beta, Q^2, x_P, t \approx 0), \quad (9)$$

so that after the integration over t , one obtains

$$f_{j/N}^{D(4)}(\beta, Q^2, x_P, t \approx 0) = B_j f_{j/N}^{D(3)}(\beta, Q^2, x_P), \quad (10)$$

where B_j is the slope of the t -dependence of $f_{j/N}^{D(4)}$. A priori there is no reason why the slope B_j should be equal for all parton flavors j and, hence, we introduce its explicit flavor dependence. In our analysis we use the following values for B_j . For all quark flavors, we use $B_q = 7.2 \pm 1.1(\text{stat.})_{-0.9}^{+0.7}(\text{syst.}) \text{ GeV}^{-2}$, which is determined by the measurement of the t -dependence of the diffractive structure function $F_2^{D(4)}$, as measured by ZEUS collaboration [34]. Of course, the diffractive slope should increase with decreasing x (diffractive cone shrinkage). However, since the experimental error of the value of B_q is large and no measurements of the x -dependence of B_q are available, any theoretically expected logarithmic increase of B_q will be within the quoted experimental errors. Hence, it is sufficient to use the x -independent B_q .

The slope of the gluon PDF, B_g , could be different from B_q . If the gluon-induced diffraction is dominated by small-size (compared to typical soft physics sizes) partonic configurations in the projectile, B_g could be as low as the slope of J/ψ diffractive production measured at HERA which is substantially lower than B_q . To reflect the uncertainties in the value of B_g we examined two scenarios: $B_g = 4 + 0.2 \ln(10^{-3}/x) \text{ GeV}^{-2}$ and $B_g = 6 + 0.25 \ln(10^{-3}/x) \text{ GeV}^{-2}$. The first one corresponds to the lower end of the values of the J/ψ photoproduction slope reported at HERA [35], while the second one is close to B_q and to the J/ψ slope reported in [36].

The analysis of the 1994 H1 data [29] showed that at large x_P , the successful fit to the data requires both the Pomeron and the Reggeon contributions. In our analysis we include only the dominant Pomeron part. The Reggeon contribution insignificantly alters our predictions for nPDFs at Bjorken x close to $x_{P,0}$, where the theoretical ambiguities are large anyway. The discussion of the Reggeon contribution can be found in the Appendix.

Using Eq. (10), the rescattering cross section σ_{eff}^j becomes

$$\sigma_{\text{eff}}^j(x, Q^2) = \frac{16\pi B_j}{f_{j/N}(x, Q^2)(1 + \eta^2)} \int_x^{x_{P,0}} dx_P f_{j/N}^{D(3)}(\beta, Q^2, x_P), \quad (11)$$

where η is the ratio of the real to imaginary parts of the diffractive amplitude \mathcal{A} . This ratio can be related to the intercept of the effective Pomeron trajectory, $\alpha_P(0)$, using the Gribov-Migdal result [37]

$$\eta = \frac{\pi}{2}(\alpha_P(0) - 1) = 0.32, \quad (12)$$

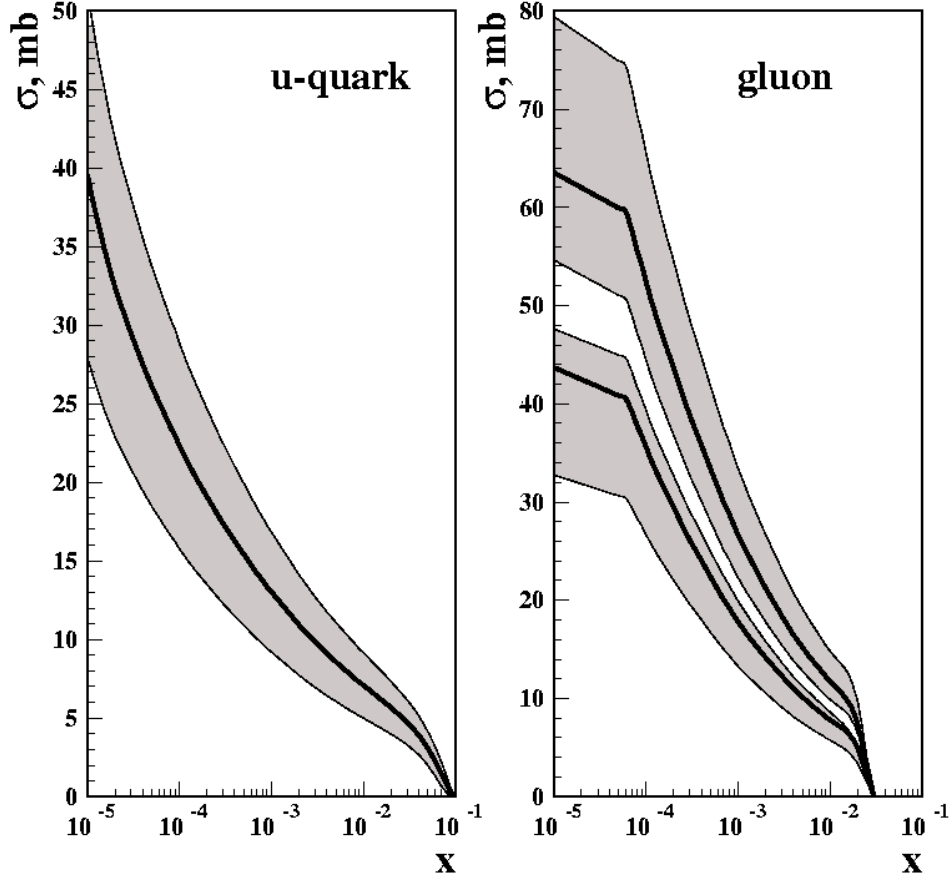


FIG. 4: The effective cross section σ_{eff} for the anti u -quark and gluon channels at $Q_0^2 = 4 \text{ GeV}^2$. The error bands represent the uncertainty in the predictions discussed in the text.

where the H1 value for $\alpha_P(0)$ was employed.

The results of the evaluation of σ_{eff}^j are presented in Fig. 4. The left panel presents σ_{eff} for anti u -quarks and the right panel is for the gluons, both cases for $Q^2 = 4 \text{ GeV}^2$. The error bands around the central curves represent the uncertainty in the determination of σ_{eff} . This uncertainty comes from the uncertainties in B_q , $f_{j/N}^{D(3)}(\beta, Q^2, x_P)$ (taken to be 25%) and the choice of $x_{P,0}$ added in quadrature. Two solid curves for the gluon case correspond to the two scenarios for the slope B_g discussed above.

Now we would like to examine which values of the diffractive masses or β contribute to σ_{eff} . At very high energies (small x), one enters the regime analogous to the triple Pomeron limit of hadronic physics, which corresponds to $\beta = Q^2/(Q^2 + M_X^2) \ll 1$. In this case, one

may need to resum logs of energy in the diffractive block (logs of β). These logarithmic effects may lead to the breakdown of the DGLAP approximation. A particular realization of this logic can be found in recent studies within the framework of Color Glass Condensate model, see e.g. [38].

To analyze at what x small β become dominant, it is convenient to introduce the ratio R defined as follows

$$R(\beta_{\max}, x) = \frac{\int_x^{x_{P,0}} dx_P f_{j/N}^{D(3)}(\beta, Q^2, x_P) \Theta(\beta_{\max} - \beta)}{\int_x^{x_{P,0}} dx_P f_{j/N}^{D(3)}(\beta, Q^2, x_P)}. \quad (13)$$

The ratio R for u -quark and gluon channels at $Q_0^2 = 4 \text{ GeV}^2$ is presented in Fig. 5. In the figure, the solid curves correspond to $\beta_{\max} = 0.5$; the dashed curves correspond to $\beta_{\max} = 0.1$; the dotted curves correspond to $\beta_{\max} = 0.01$; the dot-dashed curves correspond to $\beta_{\max} = 0.001$.

From Fig. 5 one can see how much different β -regions contribute to nuclear shadowing. For instance, taking $x = 10^{-3}$, which roughly corresponds to the smallest x which could be reached in the RHIC kinematics, one sees that large diffractive masses that correspond to $\beta \leq 0.1$ (dashed curve) contribute 20% to nuclear shadowing in the quark channel and 30% to nuclear shadowing in the gluon channel. Therefore, Fig. 5 indicates that if the Color Glass Condensate model is implemented in a way consistent with the HERA diffractive data, it predicts a very small fraction of total shadowing for the RHIC kinematic range.

For completeness, we rewrite our master equation, Eq. (6), in the form which explicitly includes the diffractive slope B_j

$$\delta f_{j/A}(x, Q^2) = \frac{A(A-1)}{2} 16 B_j \pi \mathcal{R} e \left[\frac{(1-i\eta)^2}{1+\eta^2} \int d^2b \int_{-\infty}^{\infty} dz_1 \int_{z_1}^{\infty} dz_2 \int_x^{x_{P,0}} dx_P \right. \\ \left. \times f_{j/N}^{D(3)}(\beta, Q^2, x_P) \rho_A(b, z_1) \rho_A(b, z_2) e^{ix_P m_N (z_1 - z_2)} e^{-(A/2)(1-i\eta)\sigma_{\text{eff}}^j \int_{z_1}^{z_2} dz \rho_A(b, z)} \right]. \quad (14)$$

We would like to point out that while the leading twist theory of nuclear shadowing is applicable to the partons of all flavors, see Eq. (14), using the low- x HERA diffractive data, which is heavily dominated by the Pomeron contribution, we cannot make any quantitative predictions for nuclear shadowing of the valence quarks in nuclei. Nuclear shadowing for the valence quarks is driven by the t -channel exchanges with non-vacuum quantum numbers (Reggeon contribution), whose contribution is largely lost in the kinematic region of the HERA data. In practical terms, this means that Eq. (14) should be applied to evaluate nuclear shadowing for the antiquarks and gluons only.

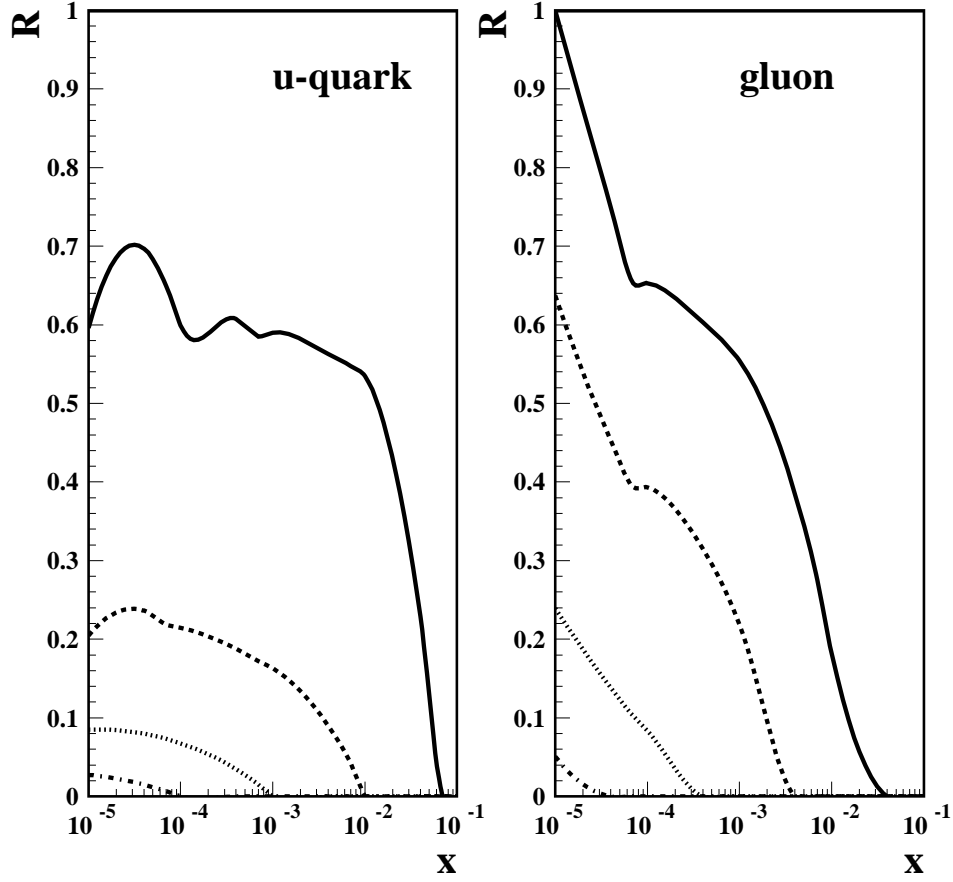


FIG. 5: The ratio R at $Q_0^2 = 4 \text{ GeV}^2$. The solid curves correspond to $\beta_{\text{max}} = 0.5$; the dashed curves correspond to $\beta_{\text{max}} = 0.1$; the dotted curves correspond to $\beta_{\text{max}} = 0.01$; the dot-dashed curves correspond to $\beta_{\text{max}} = 0.001$.

As mentioned above, Eq. (14) cannot describe nuclear modifications of PDFs at $x > 0.1$ for the quarks and $x > 0.03$ for the gluons, where nuclear antishadowing and the EMC effects dominate. For a comprehensive picture of nuclear modification for all values of x , we refer the reader to the review [15]. However, since we use Eq. (14) to evaluate nPDFs at some input scale for QCD evolution, in order to provide sensible results after the evolution, we should have a reasonable estimate of nPDFs for all x . We adopted the picture of nuclear modification of PDFs developed in [12, 39], which suggests that antiquarks in nuclei are not enhanced and the gluons are antishadowed and which uses the constraints based on the baryon and energy-momentum conservation sum rules. In our case, like in [10], we model

the enhancement of the gluon nPDF in the interval $0.03 \leq x \leq 0.2$ with a simple function $a(0.2 - x)(x - 0.03)$ and choose the free coefficient a by requiring the conservation of the momentum sum rule for nPDFs. For instance for ^{40}Ca , this requirement gives $a \approx 30$ and about 2-3% enhancement of the fraction of the total momentum of the nucleus carried by the gluons, in accord with the analysis of [12].

IV. LEADING TWIST NPDFS AND STRUCTURE FUNCTIONS

The master equation (14) allows one to determine NLO nPDFs at the input scale $Q_0^2 = 4 \text{ GeV}^2$. As an example of such a calculation, we present ratios of the nuclear (Ca-40) to free proton PDFs and the ratio of the nuclear to the free nucleon structure function, $F_2^N = (F_2^p + F_2^n)/2$, at $Q^2 = 4 \text{ GeV}^2$ by solid curves in Fig. 6. The shaded error bands around the solid curves indicate the uncertainty of the predictions. For comparison, LO predictions of Eskola *et al.* [1] (based on the LO fit to the DIS and Drell-Yan nuclear data) for the corresponding ratios are given by the dashed curves.

Note that for the gluon ratio, we give two predictions corresponding to two versions of the diffractive slope B_g discussed earlier. Also, since we do not predict nuclear shadowing for the valence quarks, this information should be taken from elsewhere. In our analysis, we use the parameterization by Eskola *et al.* [1] (see the upper left panel).

For the parameterization of the proton PDFs, we used the NLO fit CTEQ5M [40].

Figure 7 presents the Q^2 -evolution of the ratios in Fig. 6. The solid curves correspond to $Q^2 = 4 \text{ GeV}^2$; the dashed curves correspond to $Q^2 = 10 \text{ GeV}^2$; the dot-dashed curves correspond to $Q^2 = 100 \text{ GeV}^2$. The leading twist character of the predicted nuclear shadowing is apparent from this figure: the shadowing correction decreases slowly with increasing Q^2 and there is still rather significant nuclear shadowing at $Q^2 = 100 \text{ GeV}^2$.

One can see from Fig. 6 that our predictions at the lowest values of Bjorken x significantly differ from those by Eskola *et al.* However, one should keep in mind that we make our predictions to the NLO accuracy, while the fitting to the nuclear DIS data in [1] is done to the LO accuracy. One should also note that the parameterization of Eskola *et al.* [1] assumes that at small x , the ratios $F_2^A/(AF_2^N)$ and $g_A/(Ag_N)$ become equal and stay constant (saturate). We point out that:

- Figure 6 presents our predictions for the shapes of the nPDFs for ^{40}Ca , which are to

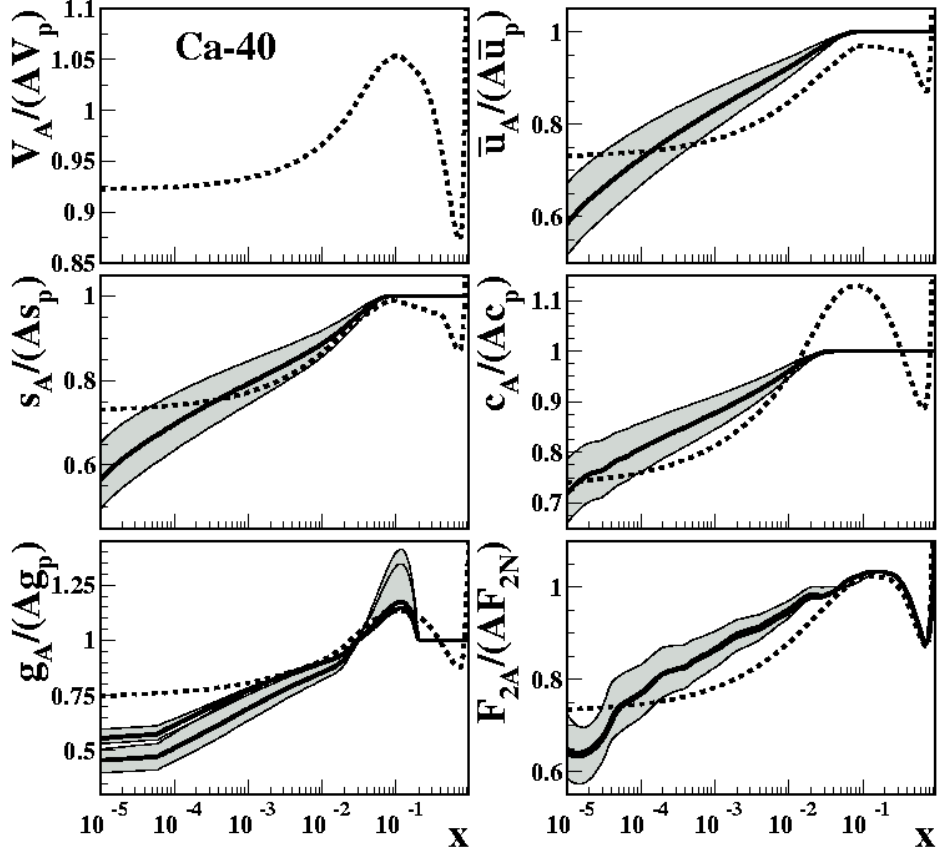


FIG. 6: The ratio of nuclear to proton NLO parton distributions and the nuclear to free nucleon inclusive structure functions F_2 in ^{40}Ca at $Q = 2$ GeV. The leading twist theory results (solid curves and the corresponded shaded error bands) are compared to the LO predictions by Eskola *et al.* [1] (dashed curves).

be used as an input for QCD evolution at the scale $Q_0 = 2$ GeV. This choice of Q_0 is motivated by the fact that the 1994 H1 diffractive data has $Q^2 \geq 4.5$ GeV² and the QCD fit to the data of [27] starts at $Q^2 = 3$ GeV². Results of such evolution are presented in Fig. 7.

- Leading twist theory predicts much more significant nuclear shadowing for quarks and gluons than the fits to the fixed-target data of Eskola *et al.* [1]. The latter *assumed* that shadowing saturates for small x , e.g. for $x \lesssim 3 \times 10^{-3}$ for ^{40}Ca , and that higher

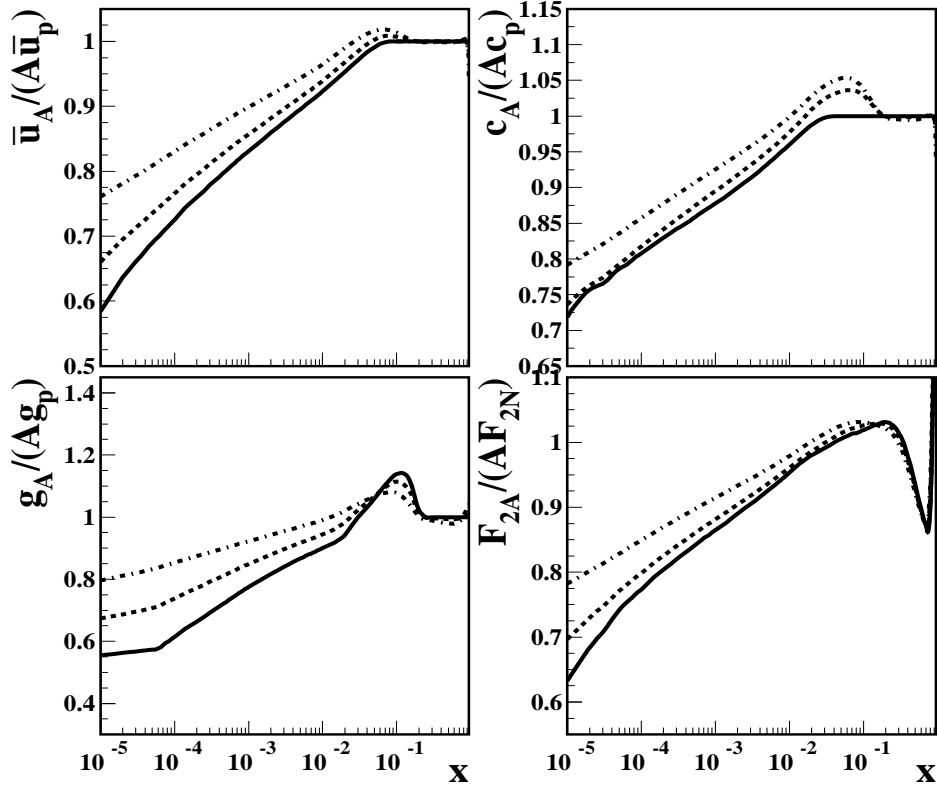


FIG. 7: Scaling violations for nuclear PDFs in ^{40}Ca . The solid curves correspond to $Q^2 = 4 \text{ GeV}^2$; the dashed curves correspond to $Q^2 = 10 \text{ GeV}^2$; the dot-dashed curves correspond to $Q^2 = 100 \text{ GeV}^2$.

twist effects are negligible.

- Nuclear shadowing for the gluons is larger than for the quarks.
- Within our model of antishadowing for the gluons by the simple function $a(0.2-x)(x-0.03)$, significant variations of the parameter a still lead to the conservation (with accuracy better than 1%) of the parton momentum sum rule. Hence, the amount of antishadowing for the gluons is not sensitive to the low- x behavior of the gluons.
- Should we compare our predictions to those by Hirai, Kumano and Miyama [2], the disagreement in the shadowing predictions would be much larger. For the comparison of the parameterizations of [1] and [2], one can consult [4].

- Comparing to the parameterization suggested in the work of Li and Wang [3], we again find a strong disagreement in the quark channel and, a surprisingly good agreement for the gluons. However, the parametrization of [3] are not based on the detailed comparison to all available fixed-target data, but rather on the need to fit the RHIC data within the HIJING model.
- The only NLO QCD fit to nuclear DIS data by de Florian and Sassot [5] produces very small nuclear shadowing for nPDFs, which is inconsistent with our predictions as well as with the predictions of [1, 2, 3].
- Our predictions for nPDFs and the structure function F_2^A for the nuclei of ^{12}C , ^{40}Ca , ^{110}Pd , ^{197}Au and ^{206}Pb and for the kinematic range $10^{-5} \leq x \leq 1$ and $4 \leq Q^2 \leq 10,000$ GeV^2 have been tabulated. They are available in the form of a simple Fortran program from V. Guzey upon request, vadim.guzey@tp2.rub.de

Nuclear shadowing corrections to nPDFs become significantly larger, when one considers the interactions with the target nucleus at small impact parameters. Indeed, since the density of nucleons in the center of the nucleus is larger than the average nucleon density, choosing small impact parameters corresponds to the increase of the number of scattering centers. Introducing the impact parameter dependent nPDFs, $f_{j/A}(x, Q^2, b)$, as was done in [10]

$$\int d^2b f_{j/A}(x, Q^2, b) = f_{j/A}(x, Q^2), \quad (15)$$

the nuclear shadowing correction to the impact parameter dependent nPDFs can be readily found from Eq. (14) by simply removing the integration over the impact parameter b

$$\begin{aligned} \delta f_{j/A}(x, Q^2, b) = & \frac{A(A-1)}{2} 16B_j \pi \mathcal{R} e \left[\frac{(1-i\eta)^2}{1+\eta^2} \int_{-\infty}^{\infty} dz_1 \int_{z_1}^{\infty} dz_2 \int_x^{x_{\mathcal{P},0}} dx_{\mathcal{P}} \right. \\ & \times f_{j/N}^{D(3)}(\beta, Q^2, x_{\mathcal{P}}) \rho_A(b, z_1) \rho_A(b, z_2) e^{ix_{\mathcal{P}} m_N (z_1 - z_2)} e^{-(A/2)(1-i\eta) \sigma_{\text{eff}}^j \int_{z_1}^{z_2} dz \rho_A(b, z)} \left. \right]. \quad (16) \end{aligned}$$

The results of the evaluation of the nuclear shadowing correction using Eq. (16) at the zero impact parameter for anti u -quarks and gluons in ^{197}Au are presented in Fig. 8 in terms of the ratios $\bar{u}_A(x, Q^2, 0)/(AT(0)\bar{u}_N(x, Q^2, 0))$ and $g_A(x, Q^2, 0)/(AT(0)g_N(x, Q^2, 0))$. The solid curves correspond to $Q^2 = 4 \text{ GeV}^2$; the dashed curves correspond to $Q^2 = 10 \text{ GeV}^2$; the dot-dashed curves correspond to $Q^2 = 100 \text{ GeV}^2$. Note that the factor $T(0) = \int dz \rho_A(b=0, z)$ provides the correct normalization of the impulse approximation term, see [10] for details.

The impact parameter-dependent nPDFs have been tabulated and are available upon request

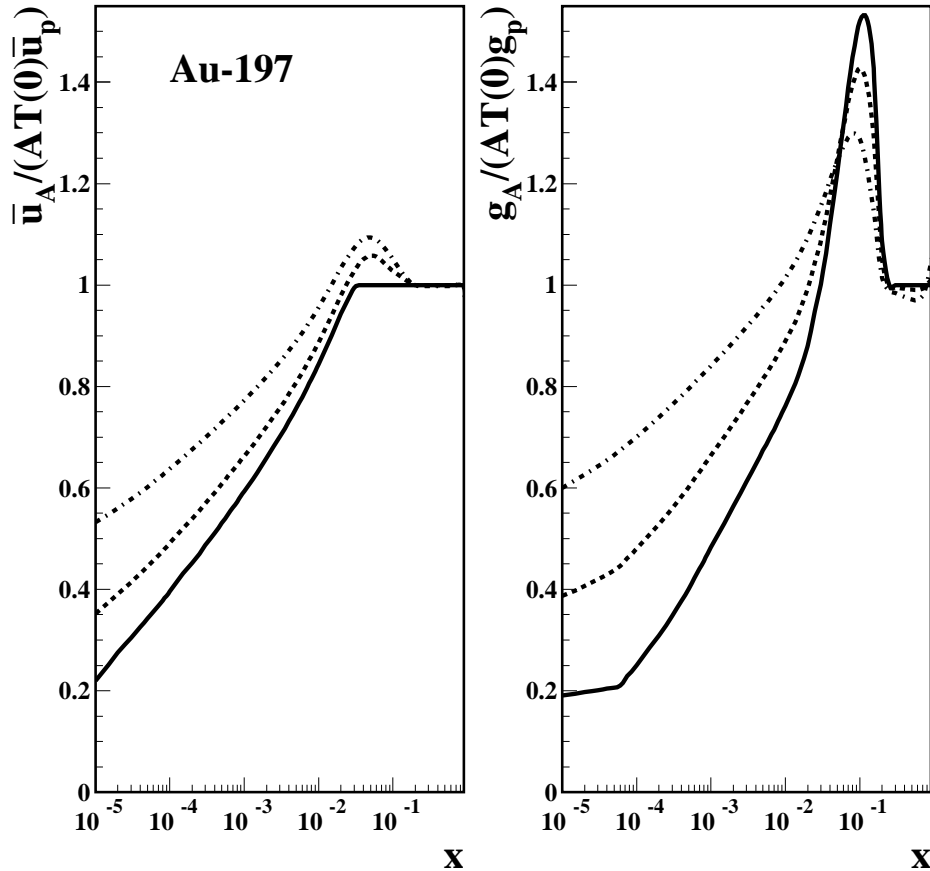


FIG. 8: Nuclear shadowing at zero impact parameter: The ratios $\bar{u}_A(x, Q^2, 0)/(AT(0)\bar{u}_N(x, Q^2, 0))$ and $g_A(x, Q^2, 0)/(AT(0)g_N(x, Q^2, 0))$ for ^{197}Au at $Q^2 = 4 \text{ GeV}^2$ (solid), $Q^2 = 10 \text{ GeV}^2$ (dashed) and $Q^2 = 100 \text{ GeV}^2$ (dot-dashed).

from V. Guzey.

V. COMPARISON TO THE DATA AND EVIDENCE FOR HIGHER TWIST EFFECTS

Our predictions for the ratio $F_2^A/(AF_2^N)$, where $F_2^N = (F_2^p + F_2^n)/2$, can be compared to the NMC data [41, 42]. However, since the low- x data points correspond to low Q^2 , we cannot make a direct comparison with those points. Therefore, we simply evaluate

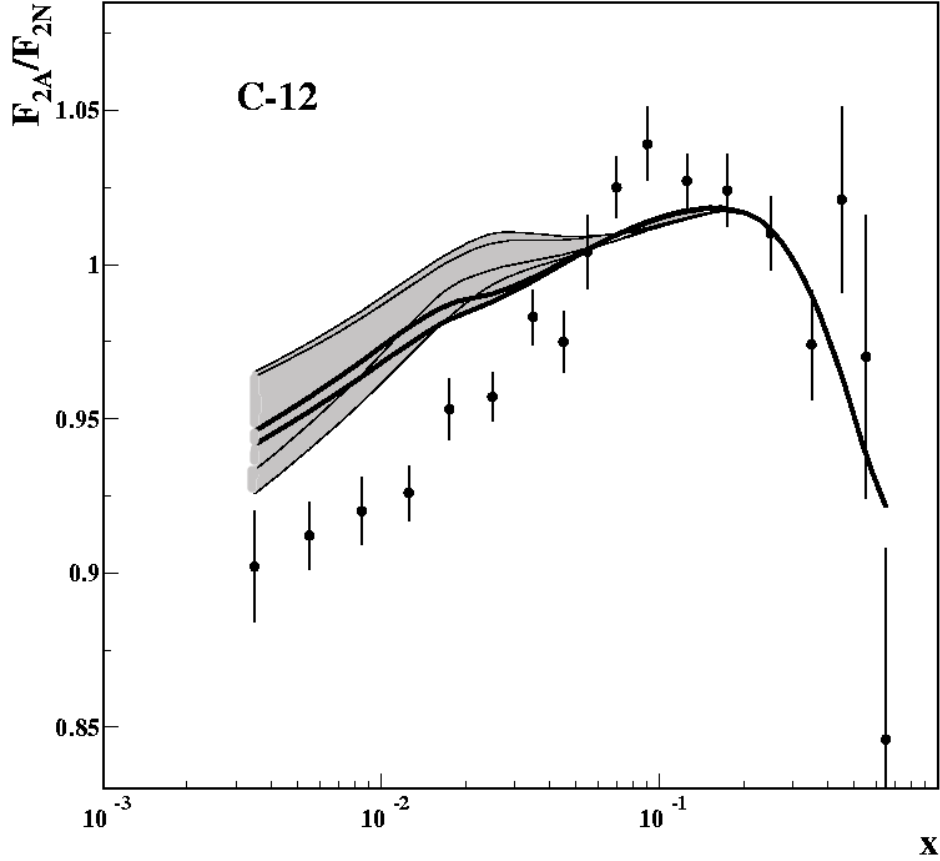


FIG. 9: Comparison of the leading twist theory results (solid curves and error bands) to the NMC data on F_2^{Ca}/F_2^N [41].

$F_2^A/(AF_2^N)$ at $Q^2 = Q_0^2 = 4 \text{ GeV}^2$ for the data points with $Q^2 < 4 \text{ GeV}^2$. Figures 9 and 10 compare our predictions (solid curves and the associated shaded error bands) to the NMC data on ^{12}C and ^{40}Ca [41]; Fig. 11 makes a comparison to the NMC $F_2^{Pb}/(F_2^C)$ ratio [42].

One can see from Figs. 9, 10 and 11 that the agreement with the data at low x is poor. Of course, one might argue that we are comparing our predictions at $Q^2 = 4 \text{ GeV}^2$ to the data with much lower Q^2 values. For instance, in Fig. 10 for the first five data points, the average values of Q^2 are $\langle Q^2 \rangle = (0.60, 0.94, 1.4, 1.9, 2.5) \text{ GeV}^2$. We have explicitly checked that the backward QCD evolution of our predictions down to $Q^2 = 2 \text{ GeV}^2$ changes the predictions only a little. Therefore, since our approach to nuclear shadowing includes the entire leading twist contribution to the nuclear shadowing correction, the disagreement with the NMC

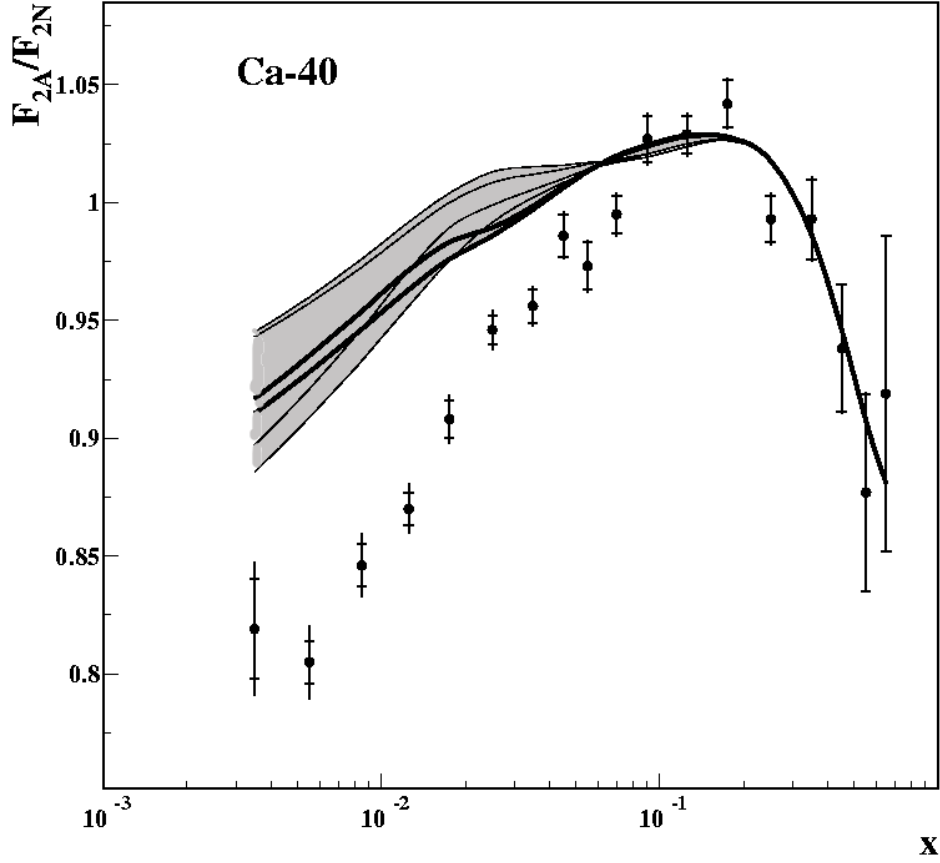


FIG. 10: Comparison of the leading twist theory results (solid curves and error bands) to the NMC data on F_2^{Ca}/F_2^N [41].

low- x data compels us to conclude that *the low- x NMC data [41, 42] contain significant higher twist effects, which contribute approximately 50% to the nuclear shadowing correction to F_2^A .*

Note that it is very natural to have rather significant higher twist effects at small Q^2 since, for this kinematics, the contribution of small diffractive masses M_X becomes important. Production of small diffractive masses M_X is dominated by the production of vector mesons, which is definitely a higher twist phenomenon. In this kinematics, the leading twist H1 parameterization of diffraction [27] underestimates by factor two the diffractive cross section as illustrated by the following estimate.

Using the definition of the diffractive differential cross section in terms of the diffractive

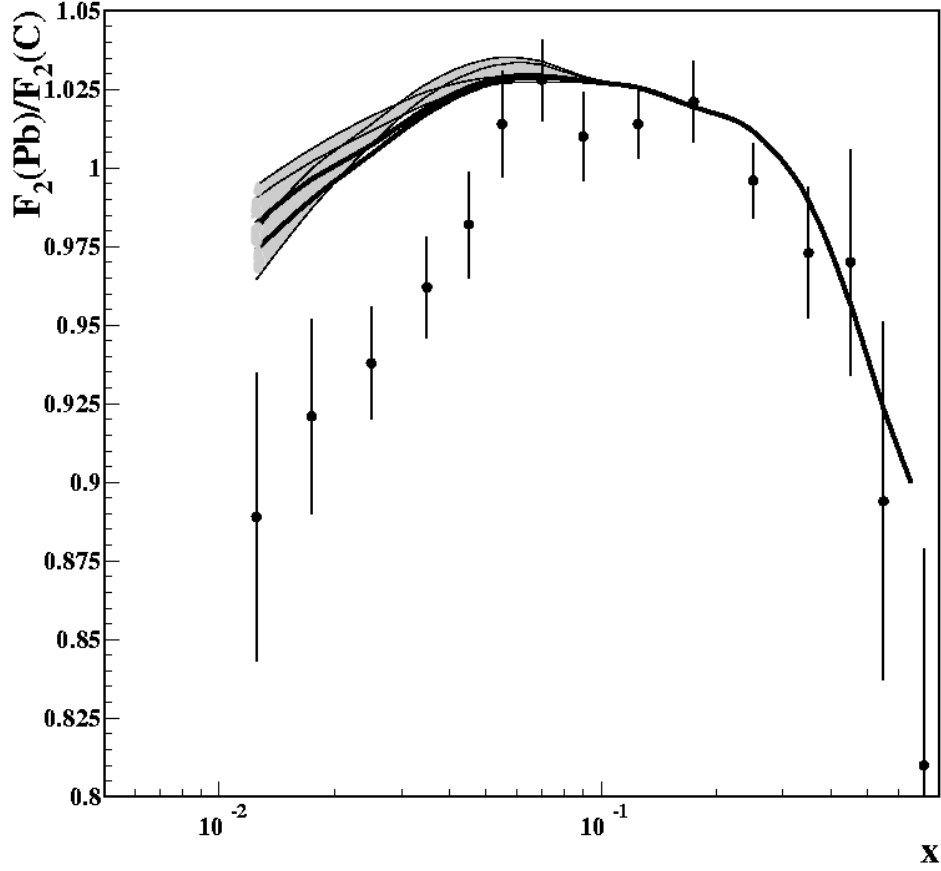


FIG. 11: Comparison of the leading twist theory results (solid curves and error bands) to the NMC data on F_2^{Pb}/F_2^C [42].

structure function $F_2^{D(3)}$ [29] and the relation between the differential cross section on the lepton level to the total cross section on the virtual photon level (the Hund convention for the virtual photon flux), $\sigma(\gamma^*p \rightarrow Xp)$, the latter can be written as

$$\sigma(\gamma^*p \rightarrow Xp) = \frac{4\pi^2\alpha_{e.m.}}{Q^2} \int_x^{x_{P,0}} dx_P F_2^{D(3)}(\beta, Q^2, x_P). \quad (17)$$

Then, if we restrict the integration in Eq. (17) by low diffractive masses M_X , $M_X \leq 1$ GeV, the resulting $\sigma(\gamma^*p \rightarrow Xp)$ can be compared to the cross section of electroproduction of vector mesons (dominated by the ρ meson). For instance, a comparison to the HERMES data on exclusive leptonproduction of ρ^0 mesons from hydrogen [43] at low Q^2 and W , $\langle Q^2 \rangle = 0.83$ GeV² and $\langle W \rangle = 5.4$ GeV, demonstrates that the calculation using Eq. (17) (with

the restriction $M_X \leq 1$ GeV) gives only 40% of the experimental value $\sigma(\gamma^*p \rightarrow \rho^0 p) = 2.04 \pm 0.10 \pm 0.43 \mu\text{b}$.

This calculation supports our conclusion about the 50% contribution of higher twist effects. Indeed, if we add to the leading twist H1 diffractive fit for $F_2^{D(3)}$ the higher twist part necessary to fit the ρ^0 leptonproduction data [43], the resulting $F_2^{D(3)}$ would results in twice as large nuclear shadowing, which would bring our predictions in Figs. 9, 10 and 11 to the agreement with the data. In this respect it is symptomatic that the disagreement is by roughly the same overall factor for all nuclei (triple rescattering in the discussed kinematics is very small as compared to the double rescattering) due to the rather large coherence length. The very same effect of the finite coherence length slows down the increase of shadowing for fixed $x \sim 0.01$ with an increase of A , see discussion in [18]. In fact, for fixed x and $A \rightarrow \infty$, nuclear shadowing asymptotically tends to a constant.

Our conclusion about the importance of the higher twist effects at small x and small Q^2 in the fixed-target data is in a broad agreement with phenomenological approaches to nuclear shadowing, which include both the scaling (leading twist) and lowest mass (ρ , ω and ϕ) vector meson (higher twist) contributions. In [13], the scaling contribution arises as the effect of the diffractive scattering, quite similarly in the spirit to the present work. However, it is difficult to assess the comparability of the pre-HERA parameterization of diffraction used in [13] with the modern HERA data on hard diffraction. More importantly, the effect of nuclear shadowing was discussed for the nuclear structure function F_2 and not for nPDFs (this comment also applies to all other work mentioned below). In other approaches, the scaling contribution results from the $q\bar{q}$ continuum of the virtual photon wave function [14], or from the contributions of higher mass vector mesons [16, 17], or from the aligned $q\bar{q}$ jets [12, 18], or from the asymmetric $q\bar{q}$ fluctuations of the virtual photon [19]. Note also that in the case of the real photon interaction with nuclei (the accurate data on the real photon diffraction for the relevant energies is available, see [44]), the shadowing data agree well with the Gribov's theory, see the discussion in Ref. [15].

We would like to point out that a fairly good description of the NMC data was achieved in [22], which uses the approach to nuclear shadowing based on its relation to diffraction on the nucleon. As an input for the their calculation, the authors used the phenomenological parameterizations of the inclusive and diffractive structure functions of the nucleon, which fit well the inclusive and diffractive data. However, in contrast to our strictly leading twist

analysis, the phenomenological parameterizations of [22] have the Q^2 -dependence of the form $(Q^2/(Q^2 + a))^b$, where a and b are numerical parameters. Hence, the analysis of [22] effectively includes higher twist contributions, which indirectly confirms our conclusion that a good description of the NMC data [41, 42] is impossible to achieve without the inclusion of the higher twist effects (contribution of vector mesons).

In addition, we would like to point to the important difference between the present analysis and the analysis of [22]. In order to evaluate nuclear shadowing as a function of Q^2 , the authors of [22] apply an equation similar in the spirit to our Eq. (14) at all Q^2 . As we explain in the end of Sect. II, the application of Eq. (14) at large Q^2 violates QCD evolution because one then ignores the proper increase of the fluctuations of σ_{eff}^j as a result of the QCD evolution. Also, neglecting proper QCD evolution, one neglects the contribution of larger x effects – antishadowing and EMC effects – to the small- x region. The second major difference is that the use of the QCD factorization theorem for hard diffraction allowed us to make predictions for nPDFs. Since this factorization theorem is not used in [22], only nuclear structure function F_2^A is considered.

Figure 12 compares our predictions for the Q^2 -dependence of the F_2^{Sn}/F_2^C ratio at $x = 0.0125$ to the NMC data [45]. At such a large value of x , we predict only a few percent shadowing correction and fail to describe the data. However, we do not claim that our approach at $x \approx 10^{-2}$ has the precision sufficient to draw any conclusions about nuclear shadowing because many other effects such as e.g. the Reggeon contribution to shadowing, not included in our formalism, begin to play an important role. Therefore, we disagree with the statement of [46] that the NMC data on the F_2^{Sn}/F_2^C ratio scaling violations constrains nuclear gluon shadowing and excludes large nuclear shadowing. Among other things this statement crucially depends on the assumption of the smallness of higher twist effects. However, higher twist effects can readily explain the pattern of nuclear shadowing observed by the NMC as being due to the vector meson contribution to shadowing, see e.g. [15].

Next we discuss the importance of the next-to-leading order (NLO) effects in the nuclear structure function F_2 . Using the LO parameterization for the ratios of the nuclear to proton PDFs of Eskola *et al.* [1] at the initial scale $Q_0 = 1.5$ GeV, we perform QCD evolution to $Q^2 = 10$ GeV² both with NLO and LO accuracy. The resulting $F_2^{Ca}/(AF_2^N)$ ratios after the NLO evolution (dashed curve) and LO evolution (dot-dashed curve) are presented in Fig. 13. For the proton PDFs, we use CTEQ5 parameterizations [40]: CTEQ5M for the

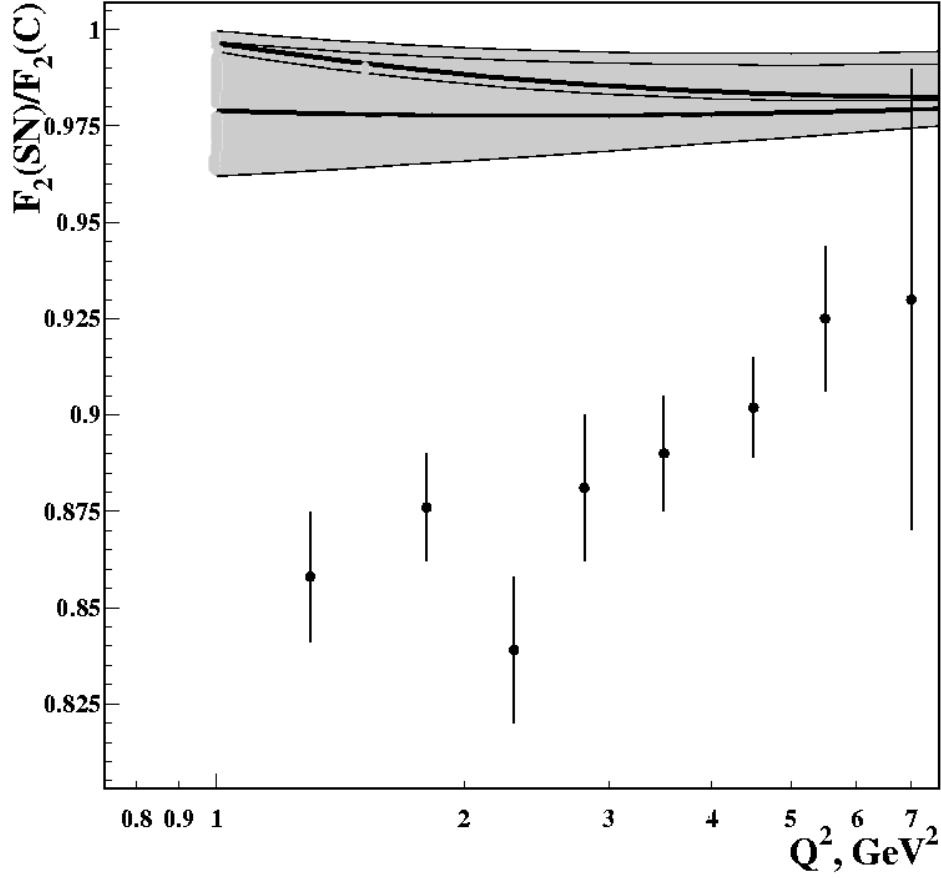


FIG. 12: Comparison of the leading twist theory results (solid curves and error bands) to the NMC data on Q^2 -dependence of F_2^{Sn}/F_2^C [45].

NLO calculations and CTEQ5L for the LO calculations. For comparison, we also present $F_2^{Ca}/(AF_2^N)$ (solid curves and the associated error bands) calculated using our leading twist model. The two solid curves correspond to the two scenarios of nuclear shadowing for gluons (two models for B_g). A significant difference between the solid and dashed curves in Fig. 13 demonstrates that the effects associated with the NLO QCD evolution and NLO expression for the structure function F_2 are important both in the very low- x region and in the x -region of the fixed-target data, $x > 0.003$. This gives us another indication that the LO fits to the fixed-target data of [1, 2, 3] must have significant intrinsic uncertainties, especially at low- x . In addition, Fig. 13 demonstrates that it is not selfconsistent to use the LO fits for nPDFs in the NLO calculations of various hard processes with nuclei, which

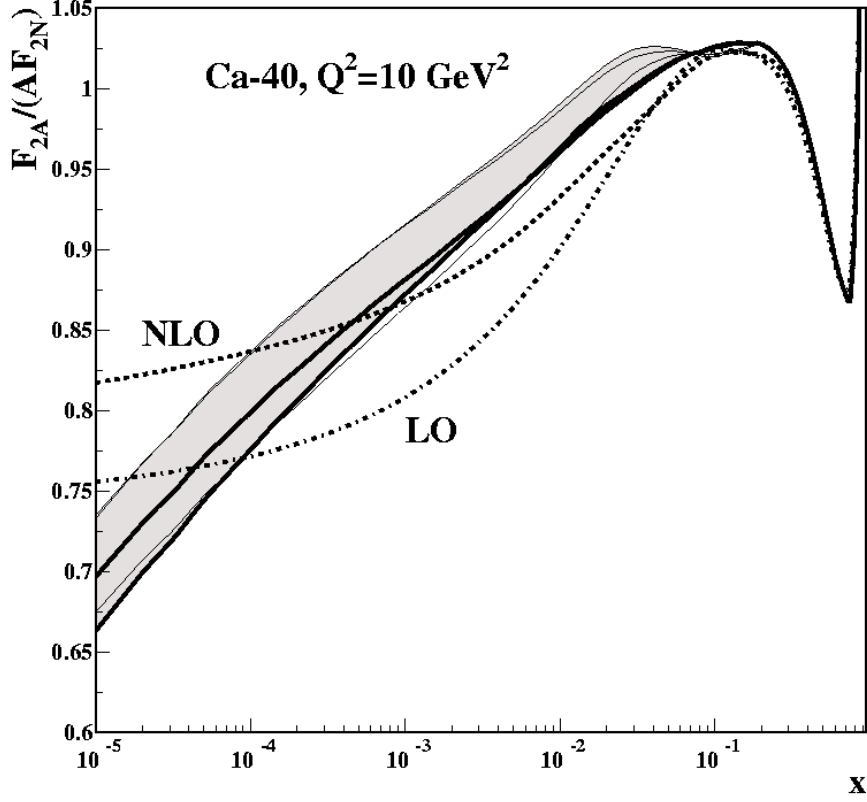


FIG. 13: LO vs. NLO evolution. The LO fits for nuclear PDFs of Eskola *et al.* [1] are evolved to $Q^2 = 10 \text{ GeV}^2$ to LO (dot-dashed curve) and to NLO (dashed curve) accuracy. Our leading twist nuclear shadowing predictions are given by the solid curves and the associated error bands.

require NLO nPDFs as an input.

VI. CONCLUSION AND DISCUSSIONS

The main results of this paper can be summarized as follows:

- We explain the derivation of the leading twist theory of nuclear shadowing in DIS on nuclei that relates nuclear shadowing in DIS on nuclei to DIS diffraction on the proton. The theory enables us to predict nuclear shadowing for individual nuclear PDFs in a model-independent way at small x , $10^{-5} \lesssim x \lesssim 10^{-2}$. At larger x , other nuclear effects (antishadowing, EMC effect) and details of the mechanism of diffraction at high x_P

introduce a certain model-dependence.

- Nuclear shadowing corrections to nPDFs are found to be large. In particular, we predict larger shadowing than given by the fits by Eskola *et al.* [1] for gluons for all x and for quarks for $x < 5 \times 10^{-4}$. In a stark disagreement with all other approaches, we predict larger nuclear shadowing for gluons than for quark.
- The presented formalism is applied to evaluate nuclear shadowing for nPDFs at all impact parameters. As one decreases the impact parameter, the effect of nuclear shadowing increases.
- Our results for the F_2^C/F_2^N , F_2^{Ca}/F_2^N and F_2^{Pb}/F_2^C ratios disagree with the corresponding fixed-target NMC data [41, 42] at low x and Q^2 . While we cannot compare our prediction directly to the data at the Q^2 values of the first five data points, we notice that the backwards QCD evolution is small and it does not seem to increase nuclear shadowing. Hence, we conclude that the NMC data with $Q^2 < 4 \text{ GeV}^2$ contain a significant amount (about 50%) of higher twist effects. This observation implies that a leading twist QCD analysis of the low- x and low- Q^2 fixed-target data will not produce reliable results for the low- x nuclear PDFs.
- Our predictions for nPDFs, impact parameter-dependent nPDFs and the structure function F_2^A for the nuclei of ^{12}C , ^{40}Ca , ^{110}Pd , ^{197}Au and ^{206}Pb and for the kinematic range $10^{-5} \leq x \leq 1$ and $4 \leq Q^2 \leq 10,000 \text{ GeV}^2$ have been tabulated. They are available in the form of a simple Fortran program from V. Guzey upon request, vadim.guzey@tp2.rub.de. The QCD evolution was carried out using the QCDNUM evolution package [47].

We must mention that there is a renewed interest in nuclear shadowing because of the recent surprising measurements of the suppression of production of hadrons with high p_t in deuteron-gold collisions at RHIC. It was claimed that the observed suppression is a spectacular confirmation of the Colored Glass Condensate model. However, in the RHIC kinematics nPDFs are probed at relatively large values of Bjorken x , on average $x > 0.01$, which is beyond the domain of the Colored Glass Condensate model. Since leading twist nuclear shadowing is rather weak for $x > 0.01$, nuclear shadowing cannot be responsible for the dramatic effect of the suppression of the hadron spectra at forward rapidities at RHIC,

see [48]. However, shadowing in the forward RHIC kinematics can be observed by selecting appropriate two jet production kinematics.

After the first version of this paper was released, there appeared an analysis [49] which calculates higher twist effects in shadowing. Similarly to us, the authors come to the conclusion that the higher twist effects in the fixed-target kinematics are large. Within uncertainties of their analysis, the higher twist effects could be even responsible for all shadowing observed at fixed target energies. So far the connection of the approach of [49] to the Gribov theory is not clear. In particular, the diagrams, which correspond to vector meson production (which dominates the higher twist small x contribution in the Gribov theory, see discussion in Sect. V) seem to be neglected as a very high twist effect.

Acknowledgments

This work was supported by the German-Israel Foundation, Sofia Kovalevskaya Program of the Alexander von Humboldt Foundation (Germany) and the Department of Energy (USA). L.F. thanks the Institute of Theoretical Physics II (Bochum) for the hospitality while this work was finished. V.G. is grateful to Ingo Bojak for his help and explanations of QCDNUM.

VII. APPENDIX

1. The analysis of the 1994 H1 data was carried out with the assumption that the diffractive structure function $F_2^{D(3)}$ is described by the sum of the effective Pomeron and Reggeon contributions [29]. The latter contribution becomes important only for large values of measured x_P , $x_P > 0.01$. Therefore, the Reggeon contribution should increase by approximately a factor of two the effect of nuclear shadowing for $x > 0.01$. However, as seen from Fig. 4 this increase is partially included in the rather large error band around the central values of σ_{eff}^j . As clearly seen from Figs. 9, 10, 11 and 12, increasing nuclear shadowing by factor two for $x > 0.01$ will lower the theoretical curves but obviously not enough to make them consistent with the data.

2. The nuclear density ρ_A , which enters the calculation of nuclear shadowing in Eq. (14), was parametrized in a two-parameter Fermi form for ^{40}Ca , ^{110}Pd , ^{197}Au and ^{206}Pb

$$\rho_A(r) = \frac{\rho_0}{1 + \exp[(r - c)/a]}, \quad (18)$$

where $r = \sqrt{|\vec{b}|^2 + z^2}$ and $a = 0.545$ fm and the parameters ρ_0 and c are presented in Table VII. Also note that $\rho_A(\vec{b}, z)$ was normalized as $2\pi \int_0^\infty d|\vec{b}| \int_{-\infty}^\infty dz |\vec{b}| \rho_A(\vec{b}, z) = 1$.

	ρ_0 (fm $^{-3}$)	c (fm)
^{40}Ca	0.0039769	3.6663
^{110}Pd	0.0014458	5.308
^{197}Au	0.000808	6.516
^{206}Pb	0.0007720	6.6178

TABLE I: The parameters entering the nuclear one-body density $\rho_A(r)$.

For ^{12}Ca , we used

$$\rho_A(r) = \rho_0 \left(1 + \alpha \left(\frac{r}{a} \right)^2 \right) e^{-r^2/a^2} \quad (19)$$

with $\rho_0 = 0.0132$, $\alpha = 1.403$ and $a = 1.635$ fm.

-
- [1] K.J. Eskola, V.J. Kolhinen and P.V. Ruuskanen, Nucl. Phys. B **535** (1998) 351; K.J. Eskola, V.J. Kolhinen and C.A. Salgado, Eur. Phys. J. C **9** (1999) 61.
- [2] M. Hirai, S. Kumano and M. Miyama, Phys. Rev. D **64** (2001) 034003.
- [3] S. Li and X.N. Wang, Phys. Lett. B **527** (2002) 85.
- [4] For a recent comparison of fits of Ref. [1] and [2], see K.J. Eskola, H. Honkanen, V.J. Kolhinen and C.A. Salgado, hep-ph/0302170.
- [5] D. de Florian and R. Sassot, Phys. Rev. D **69** (2004) 074028.
- [6] V. Guzey, *Leading twist model of nuclear shadowing*, talk at the First HERA III Workshop, Dec. 18-20, 2003, München, Germany,
<http://wwwhera-b.mppmu.mpg.de/hera3/wg2page.html>
- [7] V.N. Gribov, Sov. Phys. JETP **29** (1969) 483 [Zh. Eksp. Teor. Fiz. **56** (1969) 892].
- [8] J.C. Collins, Phys. Rev. D **57** (1998) 3051; Erratum *ibid* **61** (2000) 019902.

- [9] L. Frankfurt and M. Strikman, Eur. Phys. J. A **5** (1999) 293.
- [10] L. Frankfurt, V. Guzey, M. McDermott and M. Strikman, JHEP **202** (2002) 27.
- [11] T.H. Bauer, R.D. Spital, D.R. Yennie and F.M. Pipkin, Rev. Mod. Phys. **50** (1978) 261.
- [12] L. Frankfurt and M. Strikman, Phys. Rept. **160** (1988) 235.
- [13] W. Melnitchouk and A.W. Thomas, Phys. Rev. D **47** (1993) 3783; Phys. Lett. B **317** (1993) 437; Phys. Rev. C **52** (1995) 3373; Phys. Rev. C **67** (2003) 038201.
- [14] G. Piller, W. Ratzka and W. Weise, Z. Physik A **352** (1995) 427.
- [15] G. Piller and W. Weise, Phys. Rept. **330** (2000) 1.
- [16] J. Kwiecinski and B. Badelek, Phys. Lett. B **208** (1988) 508.
- [17] G. Shaw, Phys. Rev. D **47** (1993) R3676.
- [18] L.L. Frankfurt and M.I. Strikman, Nucl. Phys. B **316** (1989) 340.
- [19] N.N. Nikolaev and B.G. Zakharov, Phys. Lett. B **260** (1991) 414; Z. Physik **49** (1991) 607.
- [20] B. Kopeliovich and B. Povh, Phys. Lett. B **367** (1996) 329.
- [21] S.J. Brodsky and H.J. Lu, Phys. Rev. Lett. **64** (1990) 1342.
- [22] A. Capella, A. Kaidalov, C. Merino, D. Pertermann and J. Tran Thanh Van, Eur. Phys. J. C **5** (1998) 111.
- [23] L. Alvero, L. Frankfurt and M. Strikman, Eur. Phys. J. A **5** (1999) 97.
- [24] V.A. Abramovsky, V.N. Gribov and O.V. Kancheli, Yad. Fiz. **18** (1973) 595.
- [25] R.J. Glauber, Phys. Rev. **100** (1955) 242.
- [26] J.C. Collins, D.E. Soper and G. Sterman, Nucl. Phys. B **308** (1988) 833.
- [27] The FORTRAN code with the analysis of the 1994 H1 inclusive diffraction can be found at <http://www-h1.desy.de/h1/www/h1work/dif/h1994.html>.
- [28] ZEUS Collab., J. Breitweg *et al.*, Eur. Phys. J. C **6** (1999) 43.
- [29] H1 Collab., C. Adloff *et al.*, Z. Physik C **76** (1997) 613.
- [30] H1 Collab., C. Adloff *et al.*, Eur. Phys. J. C **20** (2001) 29.
- [31] L. Alvero, J.C. Collins, J. Terron and J.J. Whitmore, Phys. Rev. D **59** (1999) 074022.
- [32] F. Hautmann, Z. Kunszt and D.E. Soper, Nucl. Phys. B **563** (1999) 153.
- [33] H1 Collab., "Measurement and NLO DGLAP QCD interpretation of diffractive deep-inelastic scattering at HERA", abstract **980**, ICHEP02, July 2002, Amsterdam.
- [34] ZEUS Collab., J. Breitweg *et al.*, Eur. Phys. J. C **1** (1998) 81.
- [35] H1 Collab., C. Adloff, Phys. Lett. B **483** (2000) 23.

- [36] ZEUS Collab., A. Bruni, “*Elastic J/Ψ , $\Psi(2s)$ and Υ photoproduction at HERA*, Proc. DIS 2000, Liverpool, April 2000, eds. J.A. Gracey and T. Greenshaw (World Scientific).
- [37] V.N. Gribov and A.A. Migdal, Sov. J. Nucl. Phys. **8** (1969) 583.
- [38] L. McLerran, hep-ph/0311028.
- [39] L.L. Frankfurt, M.I. Strikman and S.Liuti, Phys. Rev. Lett. **65** (1990) 1725.
- [40] H. Lai *et al.*, Eur. Phys. J. C **12** (2000) 375.
- [41] NMC Collab., P. Amaudruz *et al.*, Nucl. Phys. B **441** (1995) 3.
- [42] NMC Collab., M. Arneodo *et al.*, Nucl. Phys. B **481**(1996) 3.
- [43] A. Airapetian *et al.* [HERMES Collab.], Eur. Phys. J. C **17** (2000) 389.
- [44] T.J. Chapin *et al.*, Phys. Rev. D **31** (1985) 17.
- [45] NMC Collab., M. Arneodo *et al.*, Nucl. Phys. B **481** (1996) 23.
- [46] K.J. Eskola, H. Honkanen, V.J. Kolhinen and C.A. Salgado, Phys. Lett. B **532** (2002) 222.
- [47] All the relevant information about the QCDNUM evolution program can be found at <http://www.nikhef.nl/~h24/qcdnum>.
- [48] W. Vogelsand, V. Guzey, and M. Strikman, in preparation.
- [49] J.-w. Qiu and I. Vitev, hep-ph/0309094.
- [50] It is possible to derive the Gribov theorem including corrections due to the real part of the diffractive amplitude (those were neglected in the Gribov’s original approach based on the Pomeron model with $\alpha_P(0) = 1$) using the Abramovskii, Gribov and Kancheli (AGK) cutting rules [24], see [9, 10]. Hence, in the small- x limit ($x \ll 10^{-2}$), the relation between shadowing and diffraction is essentially a consequence of unitarity.
- [51] The real part of the amplitude was neglected in [22], and, therefore, their corresponding expressions do not contain the factor $(1 - i\eta)^2/(1 + \eta^2)$.
- [52] The double rescattering term can be calculated using Eq. (2) at any Q^2 . However, the quasieikonal approximation employed in Eq. (6) is best justified at low $Q^2 \sim Q_0^2$, where fluctuations in the strength of the interaction are smaller (see the discussion in Ref. [10]). The QCD evolution equations automatically account for the proper increase of the fluctuations of the effective cross section around its average value σ_{eff}^j with an increase of Q^2 . This important effect is omitted if one attempts to apply Eq. (6) at $Q^2 > Q_0^2$ with a Q^2 -dependent $\sigma_{eff}^j(Q^2)$.